Multivalent Scaffolds for Affinity Maturation of Small Molecule Cell Surface Binders and Their Application to Prostate Tumor Targeting

Valerie Humblet,[#] Preeti Misra,[#] Kumar R. Bhushan,[#] Khaled Nasr,[#] Yao-Sen Ko,[§] Takashi Tsukamoto,[§] Nadine Pannier,[¶]
John V. Frangioni,*[,¶] and Wolfgang Maison*[,#]

Institute of Organic Chemistry, Justus-Liebig-Universität Giessen, Heinrich-Buff-Ring 58, 35390 Giessen, Germany, Department of Medicine and Department of Radiology, Division of Hematology/Oncology, Beth Israel Deaconess Medical Center, 330 Brookline Avenue, Boston, Massachusetts 02215, and MGI Pharma, 6611 Tributary Street, Baltimore, Maryland 21224

Received August 18, 2008

Adamantane scaffolds for affinity maturation of prostate cancer specific ligands of low molecular mass are described. These scaffolds are modular and can be used for conjugation of up to three ligands and an additional effector molecule by standard peptide coupling techniques. The potential of the scaffolds is demonstrated with the multimerization of GPI **1**, a prostate cancer specific small molecule. A detailed study of multimerized GPI conjugates with near-infrared fluorophores and their binding properties to different prostate cancer cell lines shows the specific binding of these conjugates to cell types positive for prostate specific membrane antigen (PSMA). We demonstrate that these conjugates allow the sensitive imaging of prostate cancer cells with NIR methodology and suggest that our adamantane scaffolds might be generally useful for affinity maturation of small molecules targeting cell surface epitopes.

Introduction

Finding a cure for most cancer types has been difficult and, thus far, in most cases unsuccessful. One of the major challenges in current cancer therapy is the differentiation of tumor and “normal” cells. Cancer cells are different from other cells in a number of ways, and one might target these differences for diagnostic and therapeutic purposes. In this context, cancer specific receptors, which are present ideally on the surface of cancer cells, have attracted considerable attention as tumor markers.[1,2] If conjugated to (generally unspecific) effector molecules such as contrast agents or cytotoxic moieties, ligands for cancer specific receptors can guide effectors to a tumor site and permit the sensitive detection of cancer for diagnostic purposes or the specific elimination of cancer cells for therapeutic applications.[3−6]

In contrast to monoclonal antibodies, which have been the gold standard for tumor targeting in the past,[7] small cancer-specific molecules have very favorable pharmacokinetic properties particularly for diagnostic applications where their fast blood clearance improves the signal-to-noise ratio.[8] In addition, they have better tumor penetration, are relatively easy to synthesize, and may be useful in multimodality imaging.[9] On the other hand, ligands of low molecular weight do often have inadequate binding affinity and/or specificity for a given tumor marker.

Prostate cancer is the most widely diagnosed cancer in men in the U.S., and an estimated 28 000 previously diagnosed will die of the disease in 2008.[10] In this paper, we report the application of the multimerized small molecule concept to prostate cancer imaging with targeted NIR[a] dyes. Near-infrared (700−900 nm) fluorescent light for in vivo imaging has recently received considerable interest.[11] It is invisible to the human eye but has a high transmission through living tissue. It is safe at the fluence rates used, and most tissues have low NIR autofluorescence. Targeted NIR fluorescence imaging systems are thus valuable tools for prostate cancer diagnosis and are expected to be particularly valuable for image-guided prostate cancer surgery.[11,12]

Results and Discussion

Our group[13] and others[14−16] have chosen prostate-specific membrane antigen (PSMA), a membrane bound glycoprotein,[17] as a target of choice for prostate cancer because of its transmembrane location and the fact that it is overexpressed on malignant prostate cells and their metastases.[18] Although also expressed on normal prostate epithelial cells, such normal cells are not needed after childbearing, making PSMA an ideal target.

We have previously described the development of a high-affinity (9 nM), small molecule specific for the active site of the tumor marker PSMA. This ligand, termed GPI **1**[19] (Scheme 1), was engineered to contain a primary amine for conjugation to effector molecules without losing its binding affinity for the target receptor.[13] Conjugates of GPI **1** (and other PSMA-specific small molecules) with contrast agents are therefore valuable tools for prostate tumor imaging.[16,20−23]

However, it turned out that GPI cannot effectively compete with high concentrations of endogenous phosphate, limiting its use in vivo. Although GPI **1** itself and its conjugates (like **2**) have good affinities to LNCap cells (a PSMA positive prostate cancer cell line) in phosphate free media like TBS, no binding was detected in phosphate buffer or serum (see Table 1 and

---

* To whom correspondence should be addressed. For J.V.F.: phone, +1 617-667-0692; fax, (+) 1 617-667-0981; e-mail, jfrangio@bidmc.harvard.edu. For W.M.: phone, (+) 49 641 9934330; fax, (+) 49 6441 99 19864; e-mail, wolfgang.maison@org.chemie.uni-giessen.de.

[#] Justus-Liebig-Universität Giessen.

[§] MGI Pharma.

[¶] Beth Israel Deaconess Medical Center.

[a] Abreviations: NIR, near-infrared; PSMA, prostate specific membrane antigen; PBS, phosphate buffered saline; TBS, tris(2-amino-2-(hydroxymethyl)propane-1,3-diol) buffered saline; SPECT, single photon emission computed tomography; NHS, *N*-hydroxysuccinimide; DMSO, dimethyl sulfoxide; TFA, trifluoroacetic acid; HBTU, *O*-benzotriazole-*N*,*N*,*N*′,*N*′-tetramethyluronium hexafluorophosphate; DIPEA, diisopropylethylamine; EDC, 1-ethyl-3-(3-dimethylaminopropyl)carbodiimide hydrochloride.

10.1021/jm801033c CCC: $40.75

Scheme 1[a]

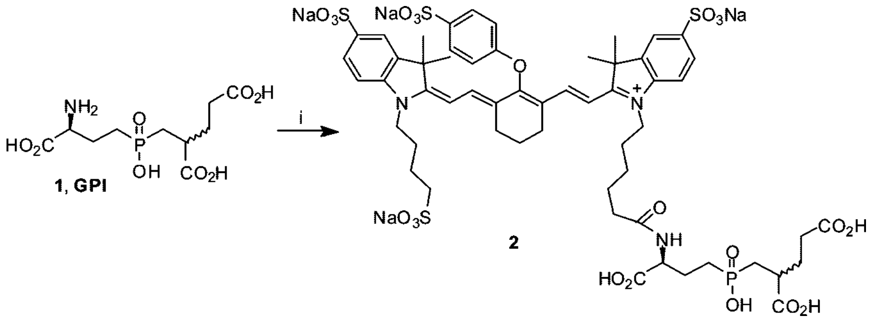

[a] Reagents and conditions: (i) Et_3N, **10a**-NHS, DMSO, 12 h, 80%.

Table 1. Live Cell Binding Affinity of PSMA Ligands for the Prostate Cancer Cell Lines LNCaP and PC3 (PSMA− and PSMA+) in Different Media

		K_d [a] (nM)		
compd	cell line	TBS	PBS	serum
1	LNCaP	10.5 ± 1.4[13]	NBD	NBD
2	LNCaP	3.6 ± 0.6	NBD	NBD
4	LNCaP	0.6 ± 0.1	0.8 ± 0.1	0.9 ± 0.1
4	PC3 (PSMA-)	NBD	NBD	NBD
4	PC3 (PSMA+)	0.2 ± 0.1	0.3 ± 0.1	0.6 ± 0.1
5	LNCaP	0.2 ± 0.1	0.3 ± 0.1	0.3 ± 0.1
5	PC3 (PSMA-)	NBD	NBD	NBD
6	LNCaP	NBD	NBD	
6	PC3 (PSMA+)	NBD	NBD	
8a	LNCaP	16.4 ± 3.1	NBD	NBD
8b	LNCaP	2.4 ± 0.7	4.8 ± 1.3	4.8 ± 1.1
8c	LNCaP	0.4 ± 0.1	0.5 ± 0.1	0.7 ± 0.1
8c	PC3 (PSMA−)	NBD	NBD	NBD
9a	LNCaP	5.4 ± 1.1	NBD	NBD
9b	LNCaP	1.3 ± 0.2	1.9 ± 0.5	1.7 ± 0.2
9c	LNCaP	0.5 ± 0.1	0.5 ± 0.1	0.4 ± 0.1
9c	PC3 (PSMA−)	NBD	NBD	NBD
10a	LNCaP	NBD		
10a	PC3 (PSMA+)	NBD		
10b	LNCaP	NBD		
10b	PC3 (PSMA+)	NBD		
11	LNCaP	0.4 ± 0.1		
11	PC3 (PSMA+)	0.5 ± 0.1		
12	LNCaP	NBD		
12	PC3 (PSMA+)	NBD		
13	LNCaP	NBD		
13	PC3 (PSMA+)	NBD		

[a] Mean ± SD. NBD: no binding detected. serum: 100% calf serum.

Figure 1). We have addressed this issue for conjugates of GPI **1** with ^{99m}Tc chelates for SPECT imaging with a multimerization approach[20] and report here on the application to prostate cancer imaging with NIR technology.

Nature often takes advantage of multimerization to decrease ligand off-rate and improve affinity of cell surface binders.[24,25] We designed suitable scaffolds for the assembly of multiple targeting ligands and contrast agents in the hope that multimerization would improve the performance of our cancer specific ligands.

Several different multivalent scaffolds have been used successfully by other groups in the past particularly for applications in carbohydrate/lectin interactions[26,27] but also for peptide/protein interactions[28] and in the context of tumor targeting.[29,30] Among these scaffolds are small molecules with few conjugation sites (~2−10) and larger systems like dendrimers[31] and polymers.[32]

We wanted to study the effect of GPI multimerization with a well defined system and focused therefore on relatively small scaffolds with few conjugation sites. For our purposes a suitable scaffold had to match certain design criteria. (1) It had to expose our ligands in the right geometry to cell surface binding epitopes. (2) It had to provide a conjugation site for contrast agents, preferably a primary amine that is compatible with well-established conjugation protocols. (3) The scaffold had to permit a rigid spacing of several highly charged ligands (GPI **1** has four negative charges) and contrast agents to avoid charge crowding that would result in problems for the conjugation of ligands or contrast agents.

Thus, we focused our attention on bridgehead functionalized adamantane as a core structure for the assembly of our multivalent imaging agents. With their rigid tetrahedral structure, these adamantane derivatives meet the above-mentioned criteria.[33] Most importantly, they provide a tripodal arrangement of tumor specific ligands using three bridgehead functionalities and an additional fourth bridgehead position for attachment of effector molecules pointing in the opposite direction. This tripodal arrangement of cell specific ligands is an ideal recognition motif for cell surfaces, as a number of receptors share a common binding motif with 3-fold geometry.[25,34−36] In addition, a number of adamantane derivatives (particularly aminoadamantanes) are well-known pharmaceuticals of low toxicity.[37,38] We have reported the use of adamantane as a multivalent scaffold in a pharmaceutical context,[20] and additional applications as a scaffold for dendritic structures and in materials science are well-known.[39−42]

In preliminary work we have shown that tetrasubstituted adamantane derivatives such as **3** (Scheme 2) can be synthesized in gram quantities and good yields from adamantane as an inexpensive starting material.[43] These tetrafunctional adamantanes have three carboxylic acids for conjugation of cancer specific ligands and a primary amine for conjugation of contrast agents. In our first experiments (Scheme 2), we conjugated GPI **1** to the Boc-protected adamantane derivative **3** and obtained the trimeric GPI conjugate **4**. The Boc group was subsequently cleaved under standard conditions with TFA, and the commercially available NIR dye **10b** was attached to the resulting free amine via NHS ester methodology. To synthesize **5**, a 10-fold excess of **10b**-NHS was necessary to obtain a decent yield. During the conjugation of NIR dye **10b**, we noticed a consistent mass loss of 136, which did not affect the fluorescence properties of the dye. We attribute this mass loss to the cleavage of a $(CH_2)_4SO_3^-$ group from **10b**.

We then tried to conjugate the commercially available tetrasulfonated NIR dye **10a** to deprotected **4**; this dye is less hydrophobic than **10b** and would be a better choice from a pharmacokinetics point of view for further in vivo investigations. The coupling yield was very low in these attempts, so we introduced a spacing moiety to avoid the steric hindrance at the amino adamantane position during

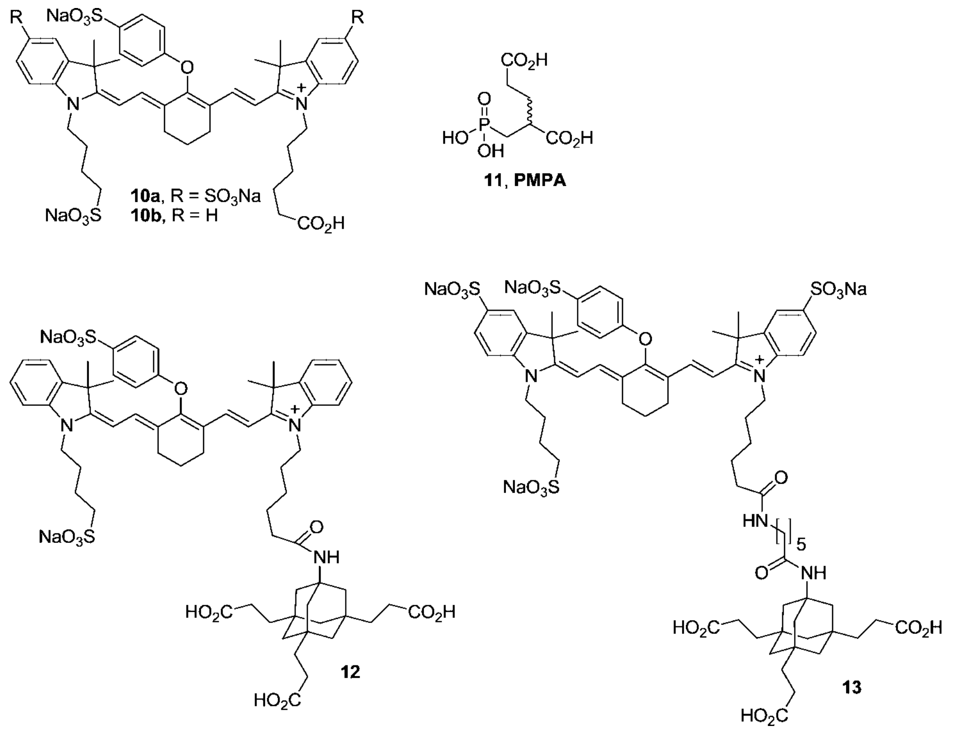

Figure 1. Compounds for control experiments listed in Table 1.

Scheme 2[a]

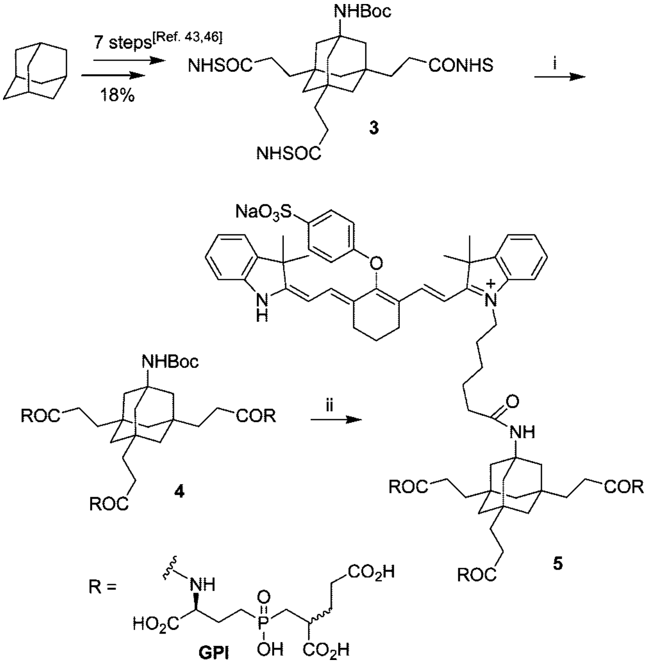

[a] Reagents and conditions: (i) Et_3N, **1**, DMSO, room temp, 18 h, 50%; (ii) (1) TFA, room temp, 5 h; (2) Et_3N, **10b**-NHS, DMSO, room temp, 18 h, two steps, 86%.

Scheme 3[a]

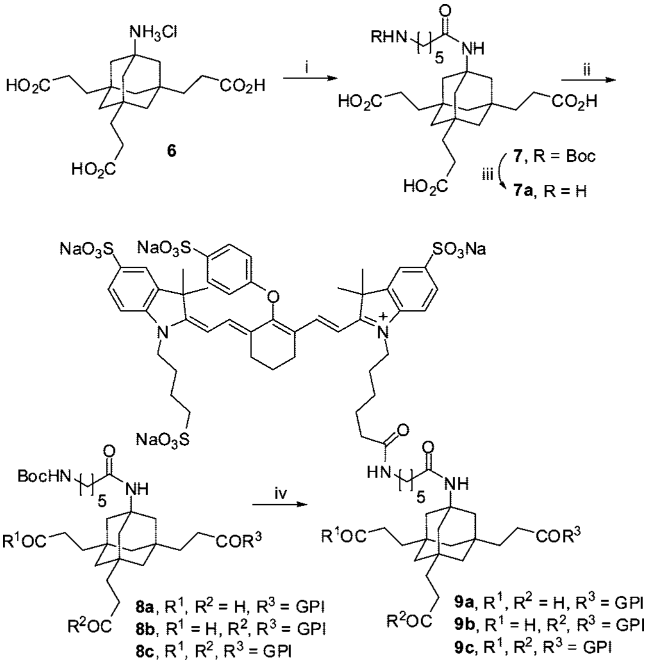

[a] Reagents and conditions: (i) (1) $TMSCH_2N_2$, room temp, 16 h, Et_3N, 74%; (2) $BocNH(CH_2)_5CO_2H$, HBTU, DIPEA, 16 h, THF, 95%; (3) LiOH, H_2O, dioxane, room temp, 20 h, 71%; (ii) (1) EDC, NHS, room temp, 12 h, 84%; (2) **1**, DMSO, room temp, 18 h. **8a**: 17%. **8b**: 25%. **8c**: 34%. (iii) TFA, room temp, 5 h; (iv) (1) TFA, room temp, 5 h; (2) Et_3N, **10a**-NHS, DMSO, room temp, 18 h, two steps each. **9a**: 19%. **9b**: 23%. **9c**: 14%.

NHS coupling. This was achieved according to Scheme 3 by transformation of triacid **6** to the corresponding trimethyl ester, which was acylated with Boc-protected γ-aminohexanoic acid and subsequently hydrolyzed with aqueous LiOH to give **7**. Conjugation to GPI **1** was done via NHS ester coupling of **7**. The coupling efficiency for this reaction is not high, and next to trimer **8c**, a significant portion of the monomeric and dimeric coupling products **8a** and **8b** were observed. This turned out to be an advantage because all three derivatives were separable by HPLC and allowed us to study the multimeric binding process systematically. In a final deprotection step the Boc group was removed with TFA to give the free primary amines, ready for conjugation to contrast agents. The NIR labeling was accomplished in one step with a 4-fold excess of **10a**-NHS ester producing compounds **9a**, **9b**, and **9c**.

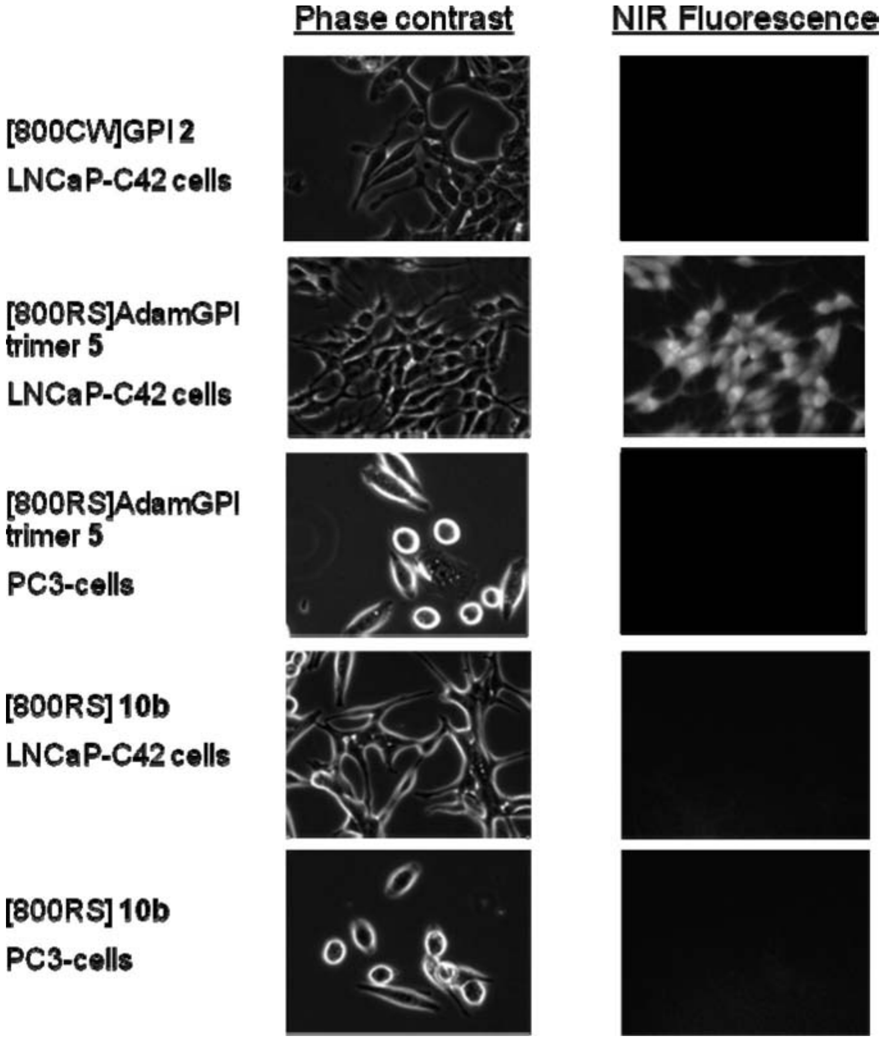

Figure 2. NIR fluorescence imaging of endogenous PSMA on living cells. Fluorescence images have identical exposure time and normalization. Shown are phase contrast (left) and NIR fluorescence (right) images. NIR fluorescence imaging of endogenous PSMA on living prostate cancer cells was first performed using PSMA-positive LNCaP cells. Cells were incubated with 2 μM compounds **2** (top row), **5** (second row), and **10b** (fourth row) in 100% calf serum for 20 min at room temperature prior to washing and image acquisition. NIR fluorescence imaging of living, PSMA-negative PC3 cells is also shown for compounds **5** (third row) and **10b** (bottom row).

The absolute affinity of each compound for the surface of living prostate cancer cells was measured using homologous competition (Table 1). In this previously described assay, ^{99m}Tc radiolabeled derivatives of the PSMA specific small molecules were used as radiotracers.[20] To show the comparability of the assay with other techniques, we used the well-known PSMA-ligand PMPA **11**[44] as a reference compound and observed affinities (400 ± 100 pM) similar to those described in the literature (275 ± 80 pM).[14]

The data from the assay using monomeric versions of GPI (**1**, **2**, **8a**, and **9a**) confirmed our finding that high concentrations of phosphate in PBS buffer and serum compete efficiently for the active site of PSMA. In contrast, dimeric GPI conjugates **8b** and **9b** and their trimeric homologues **4**, **5**, **8c**, and **9c** show almost the same binding affinities to LNCAP cells (PSMA+) in two different buffer systems and even in serum. It should be noted that affinities of PSMA ligands are not dependent on the nature of the dye or its linker moiety to the adamantane core (compare **5** and **9c**, for example). The binding affinity of the GPI conjugate **2** is increased by an order of magnitude upon trimerization with the adamantyl scaffold, leading to subnanomolar cell surface binders **4**, **5**, **8c**, and **9c** in TBS, PBS, and serum.

We performed several control experiments to confirm the specificity of our trimeric conjugates for cells expressing PSMA on their surface. As a negative control, all compounds were tested against PC3 (PSMA−) cells which do not express PSMA on their surface; no binding was detected. As a further cross-check for specificity, the trimeric conjugate **4** was also tested against PC3 (PSMA+) cells and again showed subnanomolar binding in all three media. The binding data for compounds **6**, **10a**, **10b**, **12**, and **13** show clearly that the adamantane scaffold alone (**6**), the dyes alone (**10a** and **10b**), and the conjugates of both (**12** and **13**) do not contribute significantly to the binding of our trimeric conjugates **4**, **5**, **8c**, and **9c**.

Encouraged by these positive results, we studied the binding of NIR-labeled compounds **2** and **5** to endogenous PSMA on the cell surface by in vitro NIR fluorescence imaging (Figure 2). Living cells were incubated with the molecules for 20 min at room temperature in TBS, PBS, or serum. As depicted in Figure 2 for **2** and **5**, only the multimeric versions of GPI bound to 100% of the PSMA-positive LNCaP in all conditions. This corresponds nicely with the binding data from Table 1 and allows the sensitive detection of prostate cancer cells with NIR technology. To prove the specificity of binding, we also checked all compounds using PSMA-negative PC3 cells (shown in Figure 2 for **9c**, bottom row). No binding was detected.

Conclusion

In conclusion, we have developed adamantane scaffolds for affinity maturation of PSMA-specific ligands of low molecular mass. Trimerization of our ligands allowed the sensitive and specific imaging of prostate cancer cells in serum with NIR methodology, which is particularly useful for intraoperative imaging. It is noted that our adamantane based multimerization platform has a modular character and can be conjugated to any contrast agent or cytotoxic agent via standard peptide coupling techniques. We have demonstrated this aspect with the synthesis of ^{99m}Tc-conjugated trimeric PSMA ligands for SPECT imaging of prostate cancer[20] and are currently transferring our imaging techniques to animal models.

Our adamantane scaffolds orient up to three ligands in a tripodal recognition motif and permit the conjugation of effector molecules without disturbing the binding process. Because molecular recognition via complexes of 3-fold geometry is a common feature of several important receptors, we suggest that the adamantane scaffold might be useful as a multimerization platform for addressing several other cell surface binding epitopes besides PSMA. Because it is not clear at the moment if the multimerization effect is due to multireceptor binding or to an enhancement of the local concentration of the ligand, we are currently evaluating the optimal spacer length and rigidity between the adamantane core and cell surface specific ligands.[45]

Experimental Section

Compounds **1**,[19] **3**,[43] **6**,[43,46] and **11**[44] were synthesized according to previously described procedures. The NHS esters of IRDye 800RS (**10b**) and IRDye 800CW (**10a**) were purchased from LI-COR (Lincoln, NE). All fluorophores were stored as dry powder and at −80° until use. HPLC grade triethylammonium acetate (TEAA), pH 7, was from Glen Research (Sterling, VA). HPLC grade water was from American Bioanalytic (Natick, MA). Solvents and chemicals obtained from commercial sources were analytical grade or better and used without further purification. NMR spectra were recorded on a Bruker-Karlsruhe AMX 400 spectrometer (400 MHz/100.6 MHz). Chemical shifts, δ, are represented in parts per million (ppm) and coupling constants, J, in hertz (Hz) from tetramethylsilane (TMS, 0 ppm) as the internal standard for $CDCl_3$ and residual solvent peaks for DMSO-d_6. Mass spectra were obtained with a VG/70-250F (VG analytical) instrument in FAB mode in a *p*-nitrobenzyl alcohol matrix or a Micromass LCT TOF-ES spectrometer (Waters).

[800CW]GPI (2). The 5 μL of a 30 mM solution of **1** in DMSO and 5 μL of a 200 mM solution of Et_3N in DMSO were mixed together. After 10 min, an amount of 5 μL of a 51 mM solution of IRDye 800CW-NHS ester (**10a**-NHS) in DMSO was added. The mixture was stirred for 12 h in the dark and at room temperature. The compound was purified by preparative HPLC (Symmetry column, method C, flow rate of 15 mL/min, retention time of 9.2 min). After the sample was freeze-dried, **2** was obtained as a green powder with an 80% yield. The purity of the compound was assessed by LC−MS (Symmetry column, method C, retention time of 6.1 min). ES-TOF(−): calculated m/z 1294.3 $[M + 2H]^-$; found 1294.3 $[M + 2H]^-$, 646.6 $[M + H]^{2-}/2$.

AdamGPI-Boc Trimer (4). An amount of 50 mg (0.16 mmol) of **1** dissolved in 0.4 mL of dry DMSO was added to 0.2 mL of pure Et_3N. After 10 min, a solution of **3** (15 mg, 0.02 mmol) in 0.4 mL of dry DMSO was added. The reaction mixture was stirred at room temperature overnight. The compound was purified by preparative HPLC (Symmetry column, method A, flow rate of 15 mL/min, retention time of 13.4 min). After the sample was freeze-dried, 13.3 mg (0.01 mmol, 50%) of **4** were obtained. The purity of the compound was assessed by LC−MS (Symmetry column, method A, retention time of 10.9 min). HRMS ES-TOF(−): calculated $C_{54}H_{84}N_4O_{29}P_3$ m/z 1345.4434 $[M - H]^-$; found 1345.4442 $[M - H]^-$, 672.2807 $[M - 2H]^{2-}/2$.

[800RS]AdamGPI Trimer (5). After addition of 2 mL of TFA to 13.3 mg (0.01 mmol) of **4**, the solution was stirred at room temperature for 5 h. The progress of the reaction was followed by LC−MS (SunFire column, method A, retention time of 9.2 min). After the sample was freeze-dried, an amount of 11.8 mg (0.009 mmol, 95%) of the amine as a white powder was obtained. ES-TOF(−): calculated $C_{49}H_{76}N_4O_{27}P_3$ m/z 1245.4 $[M - H]^-$; found 1245.4 $[M - H]^-$, 622.2 $[M - 2H]^{2-}$.

An amount of 5 μL of a 5 mM solution of the amine in DMSO was added to 5 μL of a 200 mM solution of Et_3N in DMSO. After 10 min, a total of 50 μL of a 5 mM solution of IRDye 800RS NHS ester in DMSO was added. The mixture was stirred overnight in the dark and at room temperature. The compound was purified by preparative HPLC (Symmetry column, method C, flow rate of 15 mL/min, retention time of 27.9 min). After the sample was freeze-dried, **5** was obtained as a green powder with a 90% yield. The purity of the compound was assessed by LC−MS (Symmetry column, method C, retention time of 21.4 min). ES-TOF(−): calculated m/z 966.4 $[M - 2H]^{2-}$; found 966.4 $[M - 2H]^{2-}$.

Boc-adamantane Triacid (7). An amount of 16 mL (32.1 mmol) of a 2 M solution of (trimethylsilyl)diazomethane in diethyl ether was added dropwise at room temperature to a solution of 2.59 g (6.41 mmol) of **6** in 50 mL of toluene/methanol (4:1). The resulting suspension was stirred for 16 h at room temperature, and 0.9 mL acetic acid was added. The reaction mixture was evaporated, and the residue was dissolved in 100 mL of 1 M aqueous NaOH. The resulting suspension was extracted three times with 100 mL of dichloromethane. The combined extracts were dried over Na_2SO_4, and the solvent was removed in vacuo to give 1.95 g (4.76 mmol, 74%) of the pure trimethylester. ^{1}H NMR ($CDCl_3$): δ 1.01 (d, 3H, $J = 11.9$ Hz), 1.07 (d, 3H, $J = 11.9$ Hz), 1.19 (s, 6H), 1.52 (dd, 6H, $J = 8.3$ Hz, $J = 10.3$ Hz), 2.25 (dd, 6H, $J = 8.3$ Hz, $J = 10.3$ Hz), 3.65 (s, 9H). ^{13}C NMR ($CDCl_3$): δ 28.2, 35.0, 35.3, 37.4, 37.5, 44.9, 45.2, 51.8, 53.8, 174.5. MS (FAB): m/z (%) = 410.2 $[M + H]^+$ (90%). Anal. ($C_{22}H_{35}NO_6$) C, H, N.

A solution of 232 mg (1.0 mmol) of 6-(Boc-amino)hexanoic acid and 410 mg (1.0 mmol) of the above-mentioned trimethyl ester in 20 mL of dry THF was treated with 0.35 mL (2.0 mmol) of diisopropylethylamine and 391 mg (1.0 mmol) of HBTU. After being stirred for 16 h at room temperature, the reaction mixture was heated at 60 °C for 90 min. Then dichlormethane and brine were added and the organic phase was washed twice with 20 mL of 1 M aqueous HCl, twice with 20 mL of 5% aqueous $NaHCO_3$, twice with 20 mL of brine, and then dried over Na_2SO_4. The solvent was removed in vacuo to give 592 mg (0.95 mmol, 95%) of the acylated trimethyl ester as a yellow oil. ^{1}H NMR ($CDCl_3$): δ 1.01 (d, 3H, $J = 12.2$ Hz), 1.13 (d, 3H, $J = 12.2$ Hz), 1.41 (s, 9H), 1.49−164 (m, 16H), 2.04 (dd, 2H, $J = 7.0$ Hz, $J = 14.5$ Hz), 2.24 (t, 6H, $J = 8.2$ Hz), 3.08 (dd, 2H, $J = 6.6$ Hz, $J = 14.5$ Hz), 3.63 (s, 9H), 4.56 (br, 1H), 5.19 (s, 1H). ^{13}C NMR ($CDCl_3$): δ 25.3, 26.4, 28.2, 28.5, 29.9, 34.9, 37.5, 40.4, 44.9, 45.2, 51.7, 53.7, 79.1, 156.1, 172.3, 174.5. MS (FAB): m/z (%) = 623.5 $[M + H]^+$ (20%). Anal. ($C_{33}H_{54}N_2O_9$) C, H, N.

A solution of 71 mg (1.7 mmol) of $LiOH\cdot H_2O$ in 10 mL of H_2O was added to a suspension of 300 mg (0.48 mmol) of the acylated trimethyl ester in 10 mL of dioxane, and the resulting solution was stirred 20 h at room temperature. The solvent was removed in vacuo, and the residue was dissolved in 20 mL of 1 M aqueous NaOH. The aqueous solution was washed twice with 20 mL of CH_2Cl_2, acidified to pH 1 with 4 M aqueous HCl, and extracted three times with 50 mL of ethyl acetate. The combined organic extracts were dried over Na_2SO_4. Evaporation of the solvent gave 258 mg of crude product that was crystallized from acetonitrile/ethyl acetate (1:2) to give 196 mg (0.34 mmol, 71%) of pure acid **7**. ^{1}H NMR (DMSO-d_6): δ 0.99 (d, 3H, $J = 12.2$ Hz), 1.04 (d, 3H, $J = 12.2$ Hz), 1.30−1.43 (m, 21H), 1.50 (s, 6H), 1.97 (t, 2H,

$J = 7.9$ Hz), 2.14 (t, 6H, $J = 8.1$ Hz), 2.87 (dd, 2H, $J = 6.7$ Hz), 6.74 (t, 1H, $J = 5.4$ Hz), 7.27 (s, 1H), 11.97 (s, 3H). ^{13}C NMR (DMSO-d_6): δ 25.2, 27.9, 28.3, 34.2, 36.1, 37.5, 44.4, 44.6, 52.5, 162.1, 171.6, 175.0. MS (FAB): *m/z* (%) = 581.5 [M + H]$^+$ (50%). Anal. ($C_{30}H_{48}N_2O_9$) C, H, N.

Boc-AdamGPI Trimer (8c). To a solution of 190 mg (0.33 mmol) of **7** and 113 mg (0.99 mmol) of *N*-hydroxysuccinimide in 10 mL of dry dioxane was added an amount of 191 mg (1.00 mmol) of 1-ethyl-3-(3-dimethylaminopropyl)carbodiimide hydrochloride at room temperature. The resulting solution was stirred at room temperature for 12 h, and then the solvents were evaporated in vacuo. The residual solid was dissolved in ethyl acetate and washed three times with water. Evaporation of the solvent gave 239 mg (0.27 mmol, 84%) of the tri-NHS ester as a colorless solid, which was used without further purification. ^{1}H NMR (CDCl$_3$): δ 1.12 (d, 3H, $J = 12.1$ Hz), 1.30−1.75 (m, 30H), 2.30 (dd, 2H, $J = 6.9$ Hz), 2.56−2.61 (m, 6H), 2.83 (br, 12H), 3.09 (t, 2H, $J = 6.0$ Hz), 4.60 (d, 1H, $J = 16.3$ Hz), 5.62−5.69 (m, 1H). ^{13}C NMR (CDCl$_3$): δ 25.4, 25.6, 25.8, 28.5, 34.9, 35.2, 36.8, 36.9, 37.5, 44.2, 44.5, 154.5, 169.4, 169.5, 172.0.

A total of 10.36 mg (0.027 mmol) of **1** dissolved in 0.9 mL of ultradry DMSO was added to 0.3 mL of 200 mM Et_3N in dry DMSO. After 10 min, a sample of 2.16 mg (0.0027 mmol) of tri-NHS ester dissolved in 0.27 mL of dry DMSO was added. The reaction mixture was stirred at room temperature overnight. The compound was purified by preparative HPLC (Sunfire column, method B, flow rate of 30 mL/min, retention time of 18.1 min). After the sample was freeze-dried, a total of 1.6 mg (0.0011 mmol, 40%) of **8c** was obtained. The purity of the compound was assessed by LC−MS (Sunfire column, method B, retention time of 10.8 min). ES-TOF(−): calculated $C_{60}H_{95}N_5O_{30}P_3$: *m/z* 1458.5 [M − H]$^-$; found 1458.5 [M − H]$^-$, 728.8 [M − 2H]$^{2-}$/2. Note: During the purification by preparative HPLC, the dimer (**8b**) and monomer (**8a**) of the molecule were also separated with retention times of 21.3 and 24.2 min, respectively. The yields were 30% and 20%, respectively. The purity was assessed by LC−MS using the conditions mentioned above. Dimer (**8b**): retention time, 11.9 min. ES-TOF(−): calculated $C_{50}H_{79}N_4O_{23}P_2$ *m/z* 1165.4 [M − H]$^-$; found 1165.4 [M − H]$^-$, 582.3 [M − 2H]$^{2-}$/2. Monomer (**8a**): retention time, 13.8 min. ES-TOF(−): calculated $C_{40}H_{63}N_3O_{16}P$ *m/z* 872.4 [M − H]$^-$; found 872.4 [M − H]$^-$.

[800CW]Adam GPI Monomer (9a). A solution of **8a** (0.4 mg, 0.0005 mmol) in 1.5 mL of TFA was stirred at room temperature for 5 h. The progress of the reaction was followed by LC−MS (SunFire column, method A, retention time of 11.8 min). After the sample was freeze-dried, 0.36 mg (95%) of the free amine as a pale-yellow powder was obtained. ES-TOF(−): calculated $C_{35}H_{55}N_3O_{14}P$ *m/z* 772.3 [M − H]$^-$; found 772.3 [M − H]$^-$.

Then 10 μL of a 10 mM solution of amine in DMSO and 10 μL of a 200 mM solution of Et_3N in DMSO were mixed together. After 10 min, a sample of 40 μL of a 11.9 mM solution of IRDye 800CW NHS ester in DMSO was added. The mixture was stirred overnight in the dark and at room temperature. The compound was purified by preparative HPLC (Sunfire column, method C, flow rate of 30 mL/min, retention time of 11.3 min). After the sample was freeze-dried, **9a** was obtained as a green powder, with a 20% yield. The purity of the compound was assessed by LC−MS (Sunfire column, method C, retention time of 7.7 min). ES-TOF(−): calculated *m/z* 1756.6 [M + 2H]$^-$; found 1756.6 [M + 2H]$^-$, 877.8 [M + H]$^{2-}$/2.

[800CW]AdamGPI Dimer (9b). A solution **8b** (1.3 mg, 0.0011 mmol) in 1.5 mL of TFA was stirred at room temperature for 5 h. The progress of the reaction was followed by LC−MS (SunFire column, method A, retention time of 10.6 min). After the sample was freeze-dried, 1.1 mg (95%) of the free amine as a pale-yellow powder was obtained. HRMS ES-TOF(−): calculated $C_{45}H_{71}N_4O_{21}P_2$ *m/z* 1065.4086 [M − H]$^-$; found 1065.4120 [M − H]$^-$.

A total of 10 μL of a 10 mM solution of the amine in DMSO was added to 10 μL of a 200 mM solution of Et_3N in DMSO. After 10 min, an amount of 40 μL of an 11.9 mM solution of IRDye 800CW NHS ester in DMSO was added. The reaction mixture was stirred at room temperature overnight and in the dark. The compound was purified by preparative HPLC (Sunfire column, method C, flow rate of 30 mL/min, retention time of 6.2 min). After the sample was freeze-dried, **9b** was obtained as a green powder (yield, 24%). The purity of the compound was assessed by LC−MS (Sunfire column, method C, retention time of 6.7 min). ES-TOF(−): calculated *m/z* 2049.6 [M + 2H]$^-$; found 1024.3 [M + H]$^{2-}$/2.

[800CW]AdamGPI Trimer (9c). A solution of **8c** (1.6 mg, 0.0011 mmol) in 1.5 mL of TFA was stirred at room temperature for 5 h. The progress of the reaction was followed by LC−MS (SunFire column, method A, retention time of 9.22 min). After the sample was freeze-dried, 1.4 mg (95%) of the free amine as a pale-yellow powder was obtained. HRMS ES-TOF(−): calculated $C_{55}H_{87}N_5O_{28}P_3$ *m/z* 1358.4750 [M − H]$^-$; found 1358.4435 [M − H]$^-$, 678.7416 [M − 2H]$^{2-}$/2.

An amount of 10 μL of a 10 mM solution of the amine in DMSO was added to 10 μL of a 200 mM solution of Et_3N in DMSO. After 10 min, an amount of 40 μL of an 11.9 mM solution of IRDye 800CW NHS ester in DMSO was added. The reaction mixture was stirred at room temperature overnight and in the dark. The compound was purified by preparative HPLC (Sunfire column, method C, flow rate of 30 mL/min, retention time of 9.4 min). After the sample was freeze-dried, **9c** was obtained as a green powder (yield, 15%). The purity of the compound was assessed by LC−MS (Sunfire column, method C, retention time of 5.8 min). ES-TOF(−): calculated *m/z* 2343.7 [M + 2H]$^-$; found 1171.4 [M + H]$^{2-}$/2.

Cell Lines. Human prostate cancer cells (PC-3 and LNCaP) were purchased from the ATCC (Manassas, VA). The cells lines were cultured at 37 °C, in a humidified atmosphere containing 5% CO_2, in RPMI 1640 medium (Mediatech Cellgro) supplemented with 10% of fetal bovine serum (Gemini Biotech Products, Woodland, CA) and 5% of penicillin/streptomycin (Cambrex Bio Science, Walkersville, MD).

Affinity Assays. The affinity assays were performed as previously described.[20] A homologous competition assay was employed using the ^{99m}Tc-labeled version as radiotracer. Cells were washed two times with ice-cold Tris-buffered saline (TBS), pH 7.4, and incubated for 20 min at 4 °C with 0.02 MBq (0.5 μCi) of radiotracer in the presence or absence of the test compound. Cells were then washed three times with TBS using a Millipore vacuum manifold (catalog no. MSVMHTS00), and the well contents were transferred directly to 12 mm × 75 mm plastic tubes placed in γ counter racks. Transfer was accomplished using a modified (Microvideo Instruments, Avon, MA) 96-well puncher (Millipore MAMP09608) and disposable punch tips (Millipore MADP19650). Well contents were counted on a model 1470 Wallac Wizard (Perkin Elmer, Wellesley, MA) 10-detector γ counter. To avoid internalization of the radioligand due to constitutive endocytosis,[13] live cell binding was performed at 4 °C, and curves were fit using Prism, version 4.0a (GraphPad, San Diego, CA), software.

In Vitro Fluorescence Study. For fluorescence study of endogenous PSMA, exponentially growing LNCaP and PC-3 cells at a confluence of 75% on glass coverslips were incubated with 0.2 mL of TBS, PBS, or 100% calf serum containing 2 μM of the compound to be tested for 20 min at room temperature. The cells were washed three times with TBS, PBS, or serum and fixed with 2% paraformaldehyde in PBS for 10 min at room temperature. The cells were then permeabilized with PBS supplemented with 0.1% Tween-20 (PBS-T). The coverslips were mounted using Fluoromount-G and imaged on a previously described four-channel NIR fluorescence microscope.[47]

Acknowledgment. We thank Barbara Clough for editing and Grisel Vasquez for administrative assistance. This work was funded by NIH Grant R01-CA-115296 and grants from the Lewis Family Fund, Ellison Foundation, Grants DAAD PPP 315-sc-ab and DFG MA 2519/3.

Supporting Information Available: General techniques, analytical data for target compounds, additional experimental procedures for all final compounds, and assay information. This material is available free of charge via the Internet at http://pubs.acs.org.

References

(1) Maison, W.; Frangioni, J. V. Improved chemical strategies for the targeted therapy of cancer. *Angew. Chem., Int. Ed.* **2003**, *42*, 4726–4728.

(2) Becker, K.-F.; Hofler, H. Mutant cell surface receptors as targets for individualized cancer diagnosis and therapy. *Curr. Cancer Drug Targets* **2001**, *1*, 121–128.

(3) Dillman, R. O. Monoclonal antibodies in the treatment of malignancy: basic concepts and recent developments. *Cancer Invest.* **2001**, *19*, 833–841.

(4) Haubner, R.; Kuhnast, B.; Mang, C.; Weber, W. A.; Kessler, H.; Wester, H.-J.; Schwaiger, M. [^{18}F]Galacto-RGD: synthesis, radiolabeling, metabolic stability, and radiation dose estimates. *Bioconjugate Chem.* **2004**, *15*, 61–69.

(5) Houshmand, P.; Zlotnik, A. Targeting tumor cells. *Curr. Opin. Cell Biol.* **2003**, *15*, 640–644.

(6) Liu, S.; Edwards, D. S. ^{99m}Tc-labeled small peptides as diagnostic radiopharmaceuticals. *Chem. Rev.* **1999**, *99*, 2235–2268.

(7) Reichert, J. M.; Valge-Archer, V. E. Development trends for monoclonal antibody cancer therapeutics. *Nat. Rev. Drug Discovery* **2007**, *6*, 349–356.

(8) Imai, K.; Takaoka, A. Comparing antibody and small-molecule therapies for cancer. *Nat. Rev. Cancer* **2006**, *6*, 714–727.

(9) Minchinton, A. I.; Tannock, I. F. Drug penetration in solid tumours. *Nat. Rev. Cancer* **2006**, *6*, 583–592.

(10) Jemal, A.; Siegel, R.; Ward, E.; Murray, T.; Xu, J.; Thun, M. J. Cancer statistics, 2007. *Ca—Cancer J. Clin.* **2007**, *57*, 43–66.

(11) Frangioni, J. V. In vivo near-infrared fluorescence imaging. *Curr. Opin. Chem. Biol.* **2003**, *7*, 626–634.

(12) Tanaka, E.; Choi, H. S.; Fujii, H.; Bawendi, M. G.; Frangioni, J. V. Image-guided oncologic surgery using invisible light: completed preclinical development for sentinel lymph node mapping. *Ann. Surg. Oncol.* **2006**, *13*, 1671–1681.

(13) Humblet, V.; Lapidus, R.; Williams, L. R.; Tsukamoto, T.; Rojas, C.; Majer, P.; Hin, B.; Ohnishi, S.; De Grand, A. M.; Zaheer, A.; Renze, J. T.; Nakayama, A.; Slusher, B. S.; Frangioni, J. V. High-affinity near-infrared fluorescent small-molecule contrast agents for in vivo imaging of prostate-specific membrane antigen. *Mol. Imaging* **2005**, *4*, 448–462.

(14) Zhou, J.; Neale, J. H.; Pomper, M. G.; Kozikowski, A. P. NAAG peptidase inhibitors and their potential for diagnosis and therapy. *Nat. Rev. Drug Discovery* **2005**, *4*, 1015–1026.

(15) Smith-Jones, P. M.; Vallabhajosula, S.; Navarro, V.; Bastidas, D.; Goldsmith, S. J.; Bander, N. H. Radiolabeled monoclonal antibodies specific to the extracellular domain of prostate-specific membrane antigen: preclinical studies in nude mice bearing LNCaP human prostate tumor. *J. Nucl. Med.* **2003**, *44*, 610–617.

(16) Banerjee, S. R.; Foss, C. A.; Castanares, M.; Mease, R. C.; Byun, Y.; Fox, J. J.; Hilton, J.; Lupold, S. E.; Kozikowski, A. P.; Pomper, M. G. Synthesis and evaluation of technetium-99m- and rhenium-labeled inhibitors of the prostate-specific membrane antigen (PSMA). *J. Med. Chem.* **2008**, *51*, 4504–4517.

(17) Mesters, J. R.; Barinka, C.; Li, W.; Tsukamoto, T.; Majer, P.; Slusher, B. S.; Konvalinka, J.; Hilgenfeld, R. Structure of glutamate carboxypeptidase II, a drug target in neuronal damage and prostate cancer. *EMBO J.* **2006**, *25*, 1375–1384.

(18) Schulke, N.; Varlamova, O. A.; Donovan, G. P.; Ma, D.; Gardner, J. P.; Morrissey, D. M.; Arrigale, R. R.; Zhan, C.; Chodera, A. J.; Surowitz, K. G.; Maddon, P. J.; Heston, W. D. W.; Olson, W. C. The homodimer of prostate-specific membrane antigen is a functional target for cancer therapy. *Proc. Natl. Acad. Sci. U.S.A.* **2003**, *100*, 12590–12595.

(19) Valiaeva, N.; Bartley, D.; Konno, T.; Coward, J. K. Phosphinic acid pseudopeptides analogous to glutamyl-gamma-glutamate: synthesis and coupling to pteroyl azides leads to potent inhibitors of folylpoly-gamma-glutamate synthetase. *J. Org. Chem.* **2001**, *66*, 5146–5154.

(20) Misra, P.; Humblet, V.; Pannier, N.; Maison, W.; Frangioni, J. V. Production of multimeric prostate-specific membrane antigen small-molecule radiotracers using a solid-phase ^{99m}Tc preloading strategy. *J. Nucl. Med.* **2007**, *48*, 1379–1389.

(21) Mease, R. C.; Dusich, C. L.; Foss, C. A.; Ravert, H. T.; Dannals, R. F.; Seidel, J.; Prideaux, A.; Fox, J. J.; Sgouros, G.; Kozikowski, A. P.; Pomper, M. G. *N*-[*N*-[(*S*)-1,3-Dicarboxypropyl]carbamoyl]-4-[^{18}F]fluorobenzyl-L-cysteine, [^{18}F]DCFBC: a new imaging probe for prostate cancer. *Clin. Cancer Res.* **2008**, *14*, 3036–3043.

(22) Foss, C. A.; Mease, R. C.; Fan, H.; Wang, Y.; Ravert, H. T.; Dannals, R. F.; Olszewski, R. T.; Heston, W. D.; Kozikowski, A. P.; Pomper, M. G. Radiolabeled small-molecule ligands for prostate-specific membrane antigen: in vivo imaging in experimental models of prostate cancer. *Clin. Cancer Res.* **2005**, *11*, 4022–4028.

(23) Pomper, M. G.; Musachio, J. L.; Zhang, J.; Scheffel, U.; Zhou, Y.; Hilton, J.; Maini, A.; Dannals, R. F.; Wong, D. F.; Kozikowski, A. P. 11C-MCG: synthesis, uptake selectivity, and primate PET of a probe for glutamate carboxypeptidase II (NAALADase). *Mol. Imaging* **2002**, *1*, 96–101.

(24) Kitov, P. I.; Bundle, D. R. On the nature of the multivalency effect: a thermodynamic model. *J. Am. Chem. Soc.* **2003**, *125*, 16271–16284.

(25) Mammen, M.; Chio, S.-K.; Whitesides, G. M. Polyvalent interactions in biological systems: implications for design and use of multivalent ligands and inhibitors. *Angew. Chem., Int. Ed.* **1998**, *37*, 2755–2794.

(26) Lundquist, J. J.; Toone, E. J. The cluster glycoside effect. *Chem. Rev.* **2002**, *102*, 555–578.

(27) Lindhorst, T. K. Artificial multivalent sugar ligands to understand and manipulate carbohydrate—protein interactions. *Top. Curr. Chem.* **2002**, *218*, 201–235.

(28) Wright, D.; Usher, L. Multivalent binding in the design of bioactive compounds. *Curr. Org. Chem.* **2001**, *5*, 1107–1131.

(29) Carlson, C.; Mowery, P.; Owen, R.; Dykhuizen, E.; Kiessling, L. Selective tumor cell targeting using low-affinity, multivalent interactions. *ACS Chem. Biol.* **2007**, *2*, 119–127.

(30) Thumshirn, G.; Hersel, U.; Goodman, S. L.; Kessler, H. Multimeric cyclic RGD peptides as potential tools for tumor targeting: solid-phase peptide synthesis and chemoselective oxime ligation. *Chem.—Eur. J.* **2003**, *9*, 2717–2725.

(31) Voegtle, F.; Richardt, G.; Werner, N. *Dendritische Moleküle*; B. G. Teubner Verlag: Wiesbaden, Germany, 2007.

(32) Haag, R.; Kratz, F. Polymer therapeutics: concepts and applications. *Angew. Chem., Int. Ed.* **2006**, *45*, 1198–1215.

(33) Newkome, G. R.; Kotta, K. K.; Moorefield, C. N. Design, synthesis, and characterization of conifer-shaped dendritic architectures. *Chem.—Eur. J.* **2006**, *12*, 3726–3734.

(34) Fournel, S.; Wieckowski, S.; Sun, W.; Trouche, N.; Dumortier, H.; Bianco, A; Chaloin, O.; Habib, M.; Peter, J. C.; Schneider, P.; Vray, B.; Toes, R. E.; Offringa, R.; Melief, C. J.; Hoebeke, J.; Guichard, G. C3-Symmetric peptide scaffolds are functional mimetics of trimeric CD40L. *Nat. Chem. Biol.* **2005**, *1*, 377–382.

(35) Gibson, S. E.; Castaldi, M. P. C3 symmetry: molecular design inspired by nature. *Angew. Chem., Int. Ed.* **2006**, *45*, 4718–4720.

(36) Wyatt, R.; Sodroski, J. The HIV-1 envelope glycoproteins: fusogens, antigens, and immunogens. *Science* **1998**, *280*, 1884–1888.

(37) Geldenhuys, W. J.; Malan, S. F.; Bloomquist, J. R.; Marchand, A. P.; Van der Schyf, C. J. Pharmacology and structure—activity relationships of bioactive polycyclic cage compounds: a focus on pentacycloundecane derivatives. *Med. Res. Rev.* **2005**, *25*, 21–48.

(38) Zah, J.; Terre'Blanche, G.; Erasmus, E.; Malan, S. F. Physicochemical prediction of a brain-blood distribution profile in polycyclic amines. *Bioorg. Med. Chem.* **2003**, *11*, 3569–3578.

(39) Newkome, G. R.; Nayak, A.; Behera, R. K.; Moorefield, C. N.; Baker, G. R. Chemistry of micelles series. 22. Cascade polymers: synthesis and characterization of four-directional spherical dendritic macromolecules based on adamantane. *J. Org. Chem.* **1992**, *57*, 358–362.

(40) Li, Q.; Jin, C.; Petukhov, P. A.; Rukavishnikov, A. V.; Zaikova, T. O.; Phadke, A.; LaMunyon, D. H.; Lee, M. D.; Keana, J. F. Synthesis of well-defined tower-shaped 1,3,5-trisubstituted adamantanes incorporating a macrocyclic trilactam ring system. *J. Org. Chem.* **2004**, *69*, 1010–1019.

(41) Menger, F. M.; Migulin, V. A. Synthesis and properties of multiarmed geminis. *J. Org. Chem.* **1999**, *64*, 8916–8921.

(42) Archibald, T. G.; Malik, A. A.; Baum, K.; Unroe, M. R. Thermally stable acetylenic adamantane polymers. *Macromolecules* **1991**, *24*, 5261–5265.

(43) Maison, W.; Frangioni, J. V.; Pannier, N. Synthesis of rigid multivalent scaffolds based on adamantane. *Org. Lett.* **2004**, *6*, 4567–4569.

(44) Jackson, P. F.; Cole, D. C.; Slusher, B. S.; Stetz, S. L.; Ross, L. E.; Donzanti, B. A.; Trainor, D. A. Design, synthesis, and biological activity of a potent inhibitor of the neuropeptidase N-acetylated alpha-linked acidic dipeptidase. *J. Med. Chem.* **1996**, *39*, 619–622.

(45) Nasr, K.; Pannier, N.; Frangioni, J. V.; Maison, W. Rigid multivalent scaffolds based on adamantane. *J. Org. Chem.* **2008**, *73*, 1056–1060.

(46) Nadine Pannier, W. M. Rigid C3-symmetric scaffolds based on adamantane. *Eur. J. Org. Chem.* **2008**, 1278–1284.

(47) Nakayama, A.; Bianco, A. C.; Zhang, C. Y.; Lowell, B. B.; Frangioni, J. V. Quantitation of brown adipose tissue perfusion in transgenic mice using near-infrared fluorescence imaging. *Mol. Imaging* **2003**, *2*, 37–49.

JM801033C